RSC Advances

PAPER

View Article Online
View Journal | View Issue

Check for updates

Cite this: *RSC Adv.*, 2025, **15**, 43808

Bridged diheteroaryl-vinylene scaffolds as novel non-fullerene acceptors: a theoretical approach

Jordan Garo,[b] Tommaso Nicolini,[a] Jean-Marc Sotiropoulos*[b] and Jean-Manuel Raimundo*[a]

Organic π-conjugated chromophores represent a unique and compelling class of materials with intrinsic properties that are highly valuable for the design and fabrication of optoelectronic devices, such as organic photovoltaic cells (OPV) and organic light-emitting diodes (OLEDs). To meet the specific performance requirements of such applications, tailored chromophores are designed and synthesized using a variety of strategies. Among these, the development of push–pull chromophores—featuring a π-conjugated spacer flanked by electron-donating and/or electron-withdrawing groups—has emerged as a key approach for tuning the bandgap and optimizing optoelectronic behavior. Recently, we have demonstrated the superior performance of novel bridged heteroaryl-vinylene scaffolds as narrow bandgap platforms for the construction of efficient push–pull chromophores. In particular, their integration with electron-deficient acceptors such as indan-1,3-dione derivatives has led to the identification of promising chromophores that outperform the classical Y6 NFA archetype. These new compounds exhibit a favorable balance of electronic and photophysical properties, underscoring their potential for application in advanced organic electronics.

Received 3rd July 2025
Accepted 3rd November 2025

DOI: 10.1039/d5ra04742k

rsc.li/rsc-advances

Open Access Article. Published on 11 November 2025. Downloaded on 5/1/2026 8:46:12 AM.
This article is licensed under a Creative Commons Attribution-NonCommercial 3.0 Unported Licence.

Introduction

Over the last few decades, considerable attention has been paid to developing strategies and approaches for reducing the energy bandgap in organic π-conjugated chromophores. The underlying motivation lies in the use of these systems, for instance, as active components in organic optoelectronic devices such as field-effect transistors, light emitting diodes, memory chips, chemical sensors, nonlinear optics and/or solar cells.[1–4] Some of these approaches involve reducing the bond-length alternation (BLA),[5] extending the π-conjugated backbone[6,7] or introducing appropriate donor (**D**)–acceptor (**A**) moieties (push–pull effect).[8] This research work focuses on the latter strategy. Indeed, the bandgap energy can be easily tuned by selecting and combining a specific electron-rich part (**D**) with an electron-deficient part (**A**) connected through a π-conjugated spacer leading to the classical **D**–π–**A** push–pull chromophores. More complex chromophore architectures can also be designed and envisioned by combining several **D**s and/or **A**s with different strengths. These push–pull compounds can be either symmetrical or asymmetrical affording **D**–π–**A**–π–**D**, **A**–π–**D**–π–**A**, $\mathbf{A_1}$–π–**D**–π–$\mathbf{A_2}$, $\mathbf{A_1}$–π–$\mathbf{A_2}$–π–**D**–π–$\mathbf{A_2}$–π–$\mathbf{A_1}$ type structures[9–11] or exhibiting various shapes (quadrupolar, tripodal *etc.*),[12] enabling finer control and tuning of the bandgap energy and optoelectronic properties of these entities. In such **D**–π–**A** chromophores strong intramolecular charge transfer (ICT) occurs due to the direct interaction between the donor and acceptor moieties through the π-conjugated spacer associated with (i) the formation of new orbitals, (ii) a net increase of the dipole moment and (iii) changes in the optical properties. The magnitude of the ICT can be expressed by two limiting resonance forms (Fig. 1). Indeed, optical excitation of the π-electrons by visible light induces charge transfer (CT) which characterizes the colour of the push–pull chromophores.

Thus, fundamental properties of the push–pull chromophores (HOMO, LUMO energy levels, CT band, carrier mobilities and dipole moment) can be easily tuned by judiciously alternating the π-conjugated spacer (π) and the **D**, **A** moieties. π-conjugated spacer engineering (nature, length, planarity, polarizability, composition) and variation in the type and strength of acceptors and donors as well as their mutual arrangement and number are essential for designing efficient

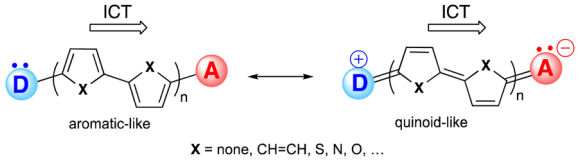

Fig. 1 General structure of linear D–π–A push–pull chromophore and its two limiting resonance forms.

[a]*Aix Marseille Univ., CNRS, CINaM, Marseille, France. E-mail: jean-manuel.raimundo@univ-amu.fr*

[b]*Universite de Pau et des Pays de l'Adour, CNRS, IPREM 5254 Pau, France. E-mail: jean-marc.sotiro@univ-pau.fr*

© 2025 The Author(s). Published by the Royal Society of Chemistry

Open Access Article. Published on 11 November 2025. Downloaded on 5/1/2026 8:46:12 AM.
This article is licensed under a Creative Commons Attribution-NonCommercial 3.0 Unported Licence.

chromophores and have been extensively developed to modulate optoelectronic properties for the foreseen applications.[13,14] Regarding the π-conjugated spacer five- and six-membered heterocycles or their fused analogues are widely used as scaffolds for the construction of push–pull chromophores. Compared to their hydrocarbon analogues they usually exhibit higher polarizability due to the presence of heteroatoms along the π-conjugated system and can act either as donor or acceptor unit. Typical donors involve chemical groups/structures possessing an electron-donating character while acceptors entail groups/structures with electron-withdrawing properties: this distinction can be qualitatively assessed through the mesomeric effect as understood in terms of resonance limit-structures. In this framework, +M (positive) effect is associated with donors while −M (negative) effect is ascribed to acceptors.[15] Among the latter, indan-1,3-dione and its derivatives[16,17] (Fig. 2) are classical electron-deficient units that have proven to be efficient for the synthesis of push–pull chromophores.

Based on these findings, linear **D**–π–**A** push–pull chromophores have been extensively developed using these indan-1,3-dione-based acceptors notably for nonlinear optical[18,19] and/or sensing[20–22] applications. More recently the replacement of the classical fullerene acceptors in organic solar cells by non-fullerene acceptors (NFAs) based on small-molecule acceptors has gained a tremendous interest due to their strong light harvesting capabilities, tunable excited state energies, and observed lower voltage loss qualities.[23] Among the various NFAs systems (**A**–π–**D**–π–**A**),-type acceptors have drawn a peculiar attention because of the high photoconversion efficiencies attained. Unfused-or fused-ring spacers (**D**) such as ITIC, BTP, ITCC, PZ *etc.*[24–29] can be used for the construction of these NFAs in combination with the indan-1,3-dione-based acceptors (**A**).[30,31] As shown by the most efficient spacers, heteroaryl-based π-conjugated systems were widely developed for such purpose leading to the highest reported photoconversion efficiencies of up to 20%.[32] However, there is still significant room for improvement at the spacer level and the challenge of identifying highly efficient spacers to construct more straightforward and powerful NFAs remains. In this context, the bridged dithienylethylene **1** (BDTE, Fig. 3) have been the focus of interest for the construction of low bandgap polymers. Compared to its non-bridged analogue (DTE) significant decrease of the oxidation potential associated with a net reduction of the BLA contribute to generate narrow bandgap polymers.[33–37] These intrinsic properties led to synthesis of efficient linear **D**–π–**A** push–pull chromophores highlighting the strong impact of the covalent rigidification concept on the linear and nonlinear optical properties.[38,39] This concept of covalent rigidification

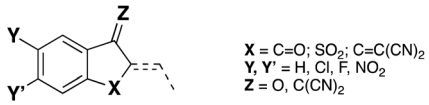

Fig. 2 Classical acceptor structures based on the indan-1,3-dione skeleton.

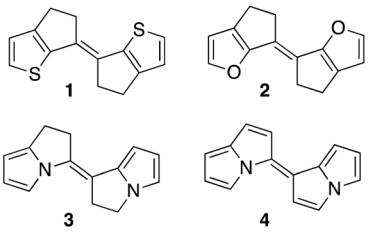

Fig. 3 Bridged diheteroaryl-vinylene scaffolds BDTE **1**–**4**.

including fused- or annulated-rings has been largely extended and adopted for the construction of other π-conjugated systems.[40] Interestingly, BDTE **1** has not been used for the construction of **A**–π–**D**–π–**A** systems although interesting features had been recently demonstrated to offer appealing opportunities.[41] In addition, we have recently shown through theoretical calculations the superiority of novel diheteroaryl-vinylene scaffolds (Fig. 3).[42]

To the best of our knowledge, none of these new scaffolds have been synthesized (except BTDE **1** and its regioisomers)[32,40] and none of them have been used for the development of (**A**–π–**D**–π–**A**)-type acceptors paving the way of novel potential classes of NFAs (Fig. 4). In addition, it is well-documented that indan-1,3-diones symmetrically substituted with halogens (F, Cl) at the 5,6-positions act as strong electron withdrawing groups and have been used for the synthesis of NFAs. In this context, 5,6-dichloro-3-oxo-2,3-dihydro-1*H*-indene-2,1-diylidene dimalononitrile and derivatives[43] in particular will serve as the basis of this study. To explore the potential of bridged heteroaryl-vinylene scaffolds, we provide an initial computational assessment of their optoelectronic properties. By applying a consistent theoretical framework, we enable systematic comparison and identification of the most promising candidates for synthesis.

Computational methods

All computations were performed in the gas phase utilizing density functional theory (DFT)[44,45] and the time-dependant

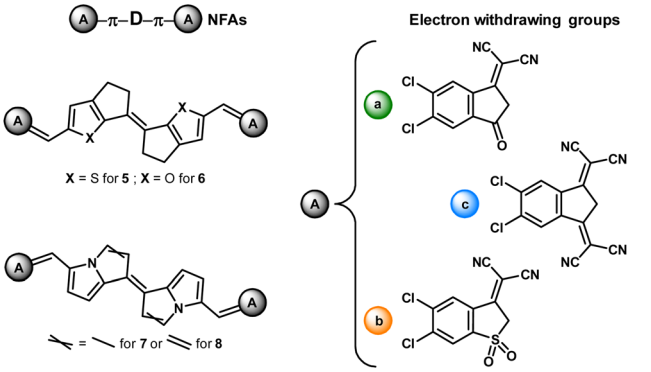

Fig. 4 Novel A–π–D–π–A-type acceptors based on bridged heteroaryl-vinylene scaffolds **1**–**4** and indan-1,3-dione-based derivatives.

Open Access Article. Published on 11 November 2025. Downloaded on 5/1/2026 8:46:12 AM. This article is licensed under a Creative Commons Attribution-NonCommercial 3.0 Unported Licence.

formalism (TDDFT)[46] is used for vertical excitation energies and photophysical properties with the Gaussian 16 package.[47] For both, the dispersion-corrected (Grimme) B3LYP-D3 (ref. 48–52) hybrid density functional comprising Becke–Johnson damping (BJ)[53] was applied in association with the triple-ζ 6-311+G(d,p)[54,55] basis set. Initially, all compounds were first subjected to optimization calculations, and confirmation that these stationary points are minima was obtained through analytical frequency calculations, with all frequencies found to be positive. After optimizing the geometries, theoretical absorption spectra and associated transitions were obtained through TDDFT calculations, considering forty singlet excited states. Triplet excited states were not considered in this initial screening, as the primary focus of our study is on the singlet optoelectronic properties relevant to photovoltaic performance. More computational details and methodologies for calculating reorganization energies, interfragmentary charge transfer (IFCT) and charge transfer matrix (CTM) are detailed in the SI. IFCT and CTM were generated with Multiwfn 3.6 (ref. 56 and 57) package while the Chemcraft[58] software was used for plotting structures and molecular orbitals.

Results and discussion

This section consists of several subsections and is structured into two main parts. First, we present the results of our calculations of key properties relevant to NFAs and we subsequently provide a detailed qualitative assessment of the expected photovoltaic performance of these novel compounds when compared to a selected, well-known NFA. Although this study focuses on 0 K geometries, finite-temperature effects (~300 K) can populate higher-energy conformers and enable vibronic pathways, potentially altering optoelectronic properties. Assessing these effects would require molecular dynamics and temperature-dependent optimizations, which we highlight as a direction for future work.

NFAs properties

Geometrical aspect. First of all, the association of donor and acceptor units raises the critical question of identifying the most stable isomers. This stability is primarily influenced by (1) the electrostatic interactions at play and (2) the steric hindrance generated, which can already be anticipated in the case of the doubly functionalized acceptor moiety **c** with malononitrile groups. For each of the 12 studied compounds, computational analysis of multiple isomers, involving variations in the dihedral angles between donor and acceptor moieties, allowed us to identify the most energetically favourable geometries (SI, Table S1).

For instance, in the case of **5a**, stabilizing electrostatic and orbital interactions[59,60] between the oxygen atom of the carbonyl group and the sulphur atom of the donor moiety seems to be favoured over the oxygen/hydrogen interaction observed in **6a**. Such non-covalent interactions are particularly valuable as they can promote planarity and consequently favour conjugation over aromaticity in π-conjugated systems.[61] In these systems, analysing structural properties such as planarity and bond lengths can provide insights into the conjugation efficiency within the studied compounds. Specifically, the values of three dihedral angles, which are directly linked to planarity, were extracted: the dihedral angle (Φ_1) within the donor moiety, and the two dihedral angles (Φ_2 and Φ_3) separating the donor and acceptor moieties (Fig. 5a). First, focusing on Φ_1, it is worth noting that despite some variability depending on the acceptor unit, all dihedral angle values remain below 1°, suggesting they have no significant impact on conjugation within the donor units. Turning to the other two dihedral angles, Φ_2 and Φ_3, optimal planarity is observed for all compounds featuring the acceptor moiety a (shown in green), with dihedral angle values ranging between 0.0° and 0.1°. For the sulfonated acceptor moiety b (in orange), a slight increase in the dihedral angles is observed, though still modest, ranging from 1.5° to 2.5° for Φ_2 and from 4.3° to 4.7° for Φ_3. A notable exception is observed for compound **8b**, where all dihedral angles are equal to 0°. Given that the only structural difference between compounds **7b** and **8b** lies in the modification of a bond within the donor moiety, it appears that the additional double bond in **8b** contributes to enhanced planarity. Finally, as expected due to the predictable steric hindrance of the malononitrile group, the most significant dihedral angle values are observed when the acceptor moiety c (in blue) is involved. Specifically, Φ_2 ranges from 9.0° to 16.8°, while Φ_3 exhibits even higher values, ranging from 14.9° to 18.7°. However, as these dihedral angles remain below 20°, the impact on conjugation should be moderate and still lie within acceptable limits. Another approach to evaluate the conjugation property within the studied compounds is the analysis of single and double bond lengths. As it is expected that single bonds shorten and double bonds lengthen with

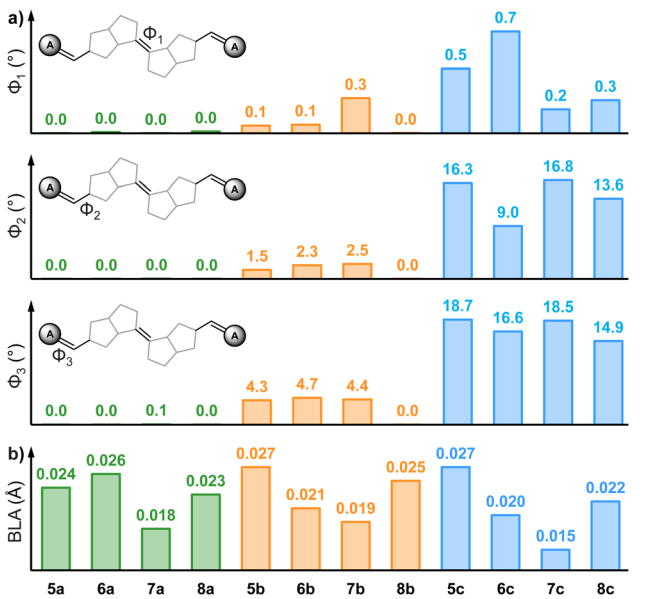

Fig. 5 Structural parameters of all compounds: (a) dihedral angle values within the donor core (Φ_1) and those (Φ_2 and Φ_3) located between the donor and acceptor moieties, in degrees. (b) Bond length alternation, in angstrom (Å).

© 2025 The Author(s). Published by the Royal Society of Chemistry

Open Access Article. Published on 11 November 2025. Downloaded on 5/1/2026 8:46:12 AM. This article is licensed under a Creative Commons Attribution-NonCommercial 3.0 Unported Licence.

increasing conjugation efficiency, the difference between the average lengths of single and double bonds should approach 0 Å. This parameter, which refers to the well-known bond length alternation (BLA), provides a quantitative measure of conjugation efficiency (Fig. 5b, see also SI Table S4 for detailed calculations).[62] From the perspective of donor moieties, a similar ranking of BLA values can be observed in compounds decorated with acceptor moieties **b** and **c**: **7** < **6** < **8** < **5**. With the exception of **6a**, the "a" series follows a similar trend, leading to the identification of nitrogen-based donor moiety **3** as the most effective in minimizing BLA regardless of acceptor unit, in contrast to BDTE **1**. On the other hand, among acceptor moieties, it can generally be established that the best BLA values are obtained for acceptor **c**, confirming the negligible impact of previous dihedral angles observed in compounds **5c–8c**.

Frontier molecular orbital. One of the most critical factors to consider, especially in OPV applications, is the impact of the design of non-fullerene acceptors on the energy levels of frontier molecular orbitals (FMOs). Since the active layer consists of donor and acceptor materials, the proper alignment of their highest occupied molecular orbital (HOMO) and the lowest unoccupied molecular orbital (LUMO) is one of the primary parameters influencing, for example, open-circuit voltage (V_{oc}), charge separation and, consequently, the performance of the cell.[63,64] First, the analysis of the FMOs reveals that the HOMO, appearing as the bonding π orbital, and the LUMO, as the antibonding one, are well-localized within the π-system of the studied compounds (SI, Table S5). Regarding the HOMO, we qualitatively observe a higher electronic density on the donor moiety compared to the acceptor moiety, while the opposite trend is observed for the LUMO. However, an exception is noted for compounds **8a**, **b**, and **c** where the electronic density remains more concentrated on the donor moiety in both FMOs. Thus, the desired push–pull effect does not appear to be optimal, which suggests that efficient charge transfer might be compromised. This aspect will be discussed in greater detail below.

In terms of FMO energy levels, the studied compounds exhibit high electron affinity, with LUMO levels below −3.9 eV, confirming their acceptor character (Fig. 6). Overall, the FMO energy levels decrease systematically with the electron-withdrawing strength of the acceptor moieties, progressing from moiety **a** to moiety **b**, and then to moiety **c**. This trend has a greater impact on the LUMO levels than on the HOMO levels. Specifically, from moiety **a** to **b** and from **b** to **c**, the LUMO energy levels decrease on average by −0.21 and −0.12 eV, respectively, compared to an average of −0.09 eV for the HOMO energy levels in both cases. When examining the influence of donor moiety on the FMO energy levels, only slight differences are observed when comparing sulphur- and oxygen-based cores, **1** and **2** respectively. From HOMO and LUMO energy levels perspective, an absolute maximum deviation of 0.08 and 0.03 eV is observed, by comparing **5a**/**6a**, **5b**/**6b** and **5c**/**6c**. Compared to the latter, the HOMO energy levels of nitrogen-containing compound series **7** appear very similar, calculated at −6.08 eV (**7a**), −6.18 eV (**7b**), and −6.22 eV (**7c**), while LUMO energy levels stand out with the highest values: −3.93 eV (**7a**), −4.20 eV (**7b**), and −4.25 eV (**7c**). Finally, with HOMO/LUMO levels of −6.29/−4.45 eV (**8a**), −6.41/−4.65 eV (**8b**), and −6.44/−4.71 eV (**8c**), the fully conjugated core of the **8** series compounds exhibits the deepest FMO energy levels among the studied systems. Based on the results obtained, it seems that the studied compounds exhibit FMOs energy levels of interest that are relatively deeper compared to those of currently developed NFAs.[65,66]

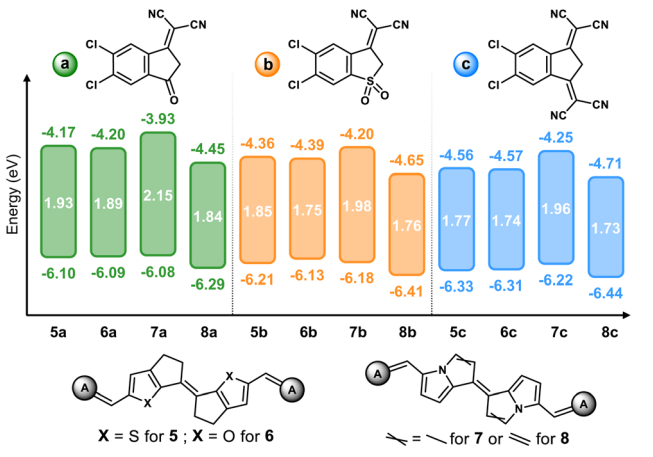

Fig. 6 Calculated HOMO and LUMO energy levels and corresponding bandgap energy ($\Delta E_{H/L}$) of all compounds.

Light absorption. Since the main envisaged application of NFAs is their use in photovoltaic devices, whose intrinsic operation mechanism is due to the interaction between photons and matter, calculating the maximum absorption wavelength (λ_{max}) and the oscillator strength (f) provides valuable insights in order to benchmark the studied compounds. In particular, NFAs development aims at obtaining efficient absorption in the 700 nm to 1100 nm wavelength range. Most importantly, the oscillator strength, empirically linked to molar extinction coefficient ε, evaluates the efficiency of light absorption, which is crucial for maximizing photon capture and thus improving cell performance. Theoretical absorption spectra calculated in the visible and near-infrared regions (600–1000 nm) qualitatively show that a single transition dominates the maximum absorption wavelength, ranging from 628 nm up to 785 nm, for all compounds (SI, Fig. S3). The analysis of these vertical transitions for each compound reveals that the optimal λ_{max} corresponds to the transition from the ground state (S_0) to the first excited state (S_1). In terms of molecular orbitals, this transition is specifically attributed to the HOMO(π) → LUMO(π^*) excitation (SI, Table S6). The moderate oscillator strengths observed across the series suggest suppressed radiative recombination, aligning with the requirement for poor fluorescence qualities in efficient NFA-based OPVs. The f *vs.* λ_{max} plot reported in Fig. 7 shows calculated values for all compounds, color-coded according to the three investigated acceptor moieties: more specifically, the green region corresponds to moiety **a**, the orange region to **b**, and blue region to **c**.

Considering the considerations discussed above regarding f and λ_{max} and their impact on NFA performance in an OPV device in terms of light absorption properties, the most promising materials should be positioned in the top-right corner of the graph. A clear trend is easily identified: a redshift in λ_{max}

Open Access Article. Published on 11 November 2025. Downloaded on 5/1/2026 8:46:12 AM.
This article is licensed under a Creative Commons Attribution-NonCommercial 3.0 Unported Licence.

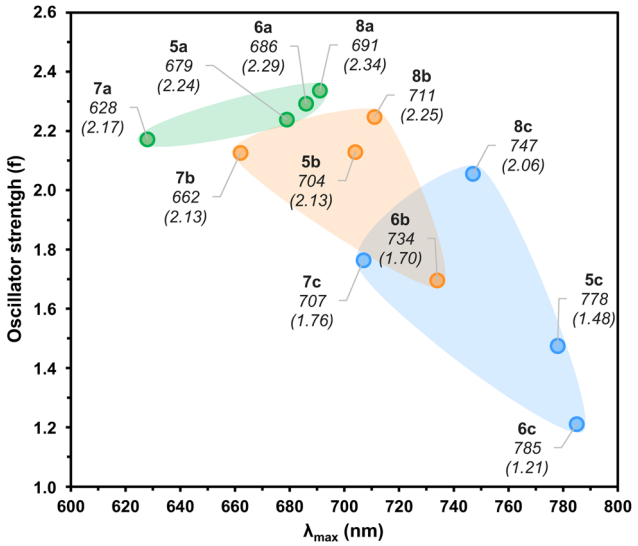

Fig. 7 Calculated maximum absorption wavelength (λ_{max}) corresponding to $S_0 \rightarrow S_1$ vertical transitions and their associated oscillator strength (f). λ_{max} and f labels in italic and brackets, respectively.

accompanied by a decrease in oscillator strength going from the carbonyl-based acceptor moiety **a** to the sulfonated moiety **b**, and then to the fully cyano-substituted moiety **c**. The average values of λ_{max} and f for each acceptor moiety reveal the following trends: **a** (671 nm) < **b** (703 nm) < **c** (754 nm) for λ_{max}, and **c** (1.63) < **b** (2.05) < **a** (2.26) for f (see SI, Table S6). Interestingly, despite the substantial deviation from planarity, evidenced by dihedral angle analysis shown earlier, compound **8c** presents the third largest absorption wavelength across the **8**-compound series. From the perspective of donor moieties, the average values of λ_{max} and f yield the following rankings: **7** (666 nm) < **8** (716 nm) < **5** (720 nm) < **6** (735 nm) for λ_{max}, and **6** (1.73) < **5** (1.95) < **7** (2.02) < **8** (2.22) for f. This indicates that the nitrogen-containing cores **7** and **8** tend to favour photon absorption efficiency, whereas the sulphur-containing core **5** and oxygen-containing core **6** are associated with the highest λ_{max} values. A rough quantitative comparison among all compounds can be obtained by defining the product $\lambda_{max} \cdot f$ as a figure of merit. According to this metric, the series **8** compounds appear to be to the most promising in terms of light absorption properties, as evidenced by the following ranking according to $\lambda_{max} \cdot f$ values normalized to 1: **8a** (1.00) > **8b** (0.99) > **6a** (0.97) > **8c** (0.95) > **5a** (0.94) > **5b** (0.93) > **7b** (0.87) > **7a** (0.84) > **7c** (0.77) = **6b** (0.77) > **5c** (0.71) > **6c** (0.59). Nonetheless, compounds **6a**, **5a**, and **5b** show relatively high values while series **7** compounds fall at still relevant values (normalized $\lambda_{max} \cdot f \geq 0.77$). However, other relevant parameters will be evaluated in the sections to allow a proper assessment of the potential of all compounds to improve performance in OPV devices.

Charge transfer. Charge transfer processes, with their complex influence on optical and electronic properties at both the molecular and active layer scales, remain a topic of debate. However, advances brought forth by the development of **Y6** as a NFA have highlighted their role in the performance of NFAs, particularly in explaining the success of this **A**–π–**D**–π–**A** archetype.[67] For **A**–π–**D**–π–**A** type NFAs, where the LUMO is localized on the terminal acceptor moieties, studying intramolecular charge transfer is crucial. This analysis aims to confirm the polarization from the donor to the terminal acceptors, which helps retain the electron on the LUMO after exciton dissociation, facilitating its transfer to the electrodes while minimizing intramolecular recombination. Charge transfer matrices (CTMs) provide a detailed visualization of charge transfers occurring between atoms (Table 1). While fragment-based pairwise CTMs can simplify analysis, we opted for an atom-wise $N \times N$ representation to capture subtle electron–hole delocalization patterns that might be overlooked in a coarse-grained approach. Partial charges were considered in the normalization, ensuring the matrices are properly scaled. Future work could explore fragment-level simplifications for larger systems. Carbon (C), nitrogen (N), oxygen (O), sulphur (S), and chlorine (Cl) atoms are symmetrically listed from one end of the molecule to the other (see SI, Table S1 for details). This arrangement ensures that the central region of the matrices corresponds to the donor moiety (**D**), while the extremities are associated with the acceptor moieties (**A**). Specifically, the first two and last two numbered atoms represent the four chlorine atoms located at the terminal positions of the compounds. As hydrogen atoms do not contribute to charge transfer, they have been omitted to enhance the clarity of the matrices. As hydrogen atoms do not significantly contribute to charge transfer, they have been omitted to enhance the clarity of the matrices. Additionally, magenta lines indicate the boundary between the donor and acceptor moieties, corresponding to the single bond adjacent to the donor moiety. Based on the structure of the matrices, the predominant and common charge transfer across all compounds is observed in the central column of the matrices. This corresponds to the transfer from the two carbon atoms of the central double bond in the donor motif (**D**) to the carbon atom in the acceptor motif (**A**) near the π-boundary with **D**. Then, three distinct groups can be identified, ranked from the least to the most efficient charge transfer: the first group includes compounds **8a** and **8b**, the second consists of those with acceptor motif **c** (**5c**–**8c**), and the final group comprises the six remaining compounds (**5a**, **5b**, **6a**, **6b**, **7a**, **7b**). The first group is characterized by density spots primarily localized along the horizontal central zone, particularly near the magenta lines referring to the π-boundaries.

This indicates charge transfers both from **A** and **D** towards these boundaries and within **D** itself. In the second group, compounds with acceptor moiety c exhibit less concentrated charge transfer near the π-boundaries and a reduced transfer from **A** to **D**. This is evidenced by significantly smaller density spots in the left and right columns of the matrices. Finally, the last group shows the most interesting pattern, with relatively high-density spots in the middle of the upper and lower sections of the central column. This reflects substantial charge transfers from **D** to **A**, specifically from the carbon atoms of the central double bond in **D** to the carbon atoms of the double bond bearing the malononitrile group in **A**. While such transfers are also observed in the first two groups, they occur on a much

© 2025 The Author(s). Published by the Royal Society of Chemistry

Open Access Article. Published on 11 November 2025. Downloaded on 5/1/2026 8:46:12 AM.
This article is licensed under a Creative Commons Attribution-NonCommercial 3.0 Unported Licence.

Table 1 Charge transfer matrix (CTM) calculated using Multiwfn. The atoms are numbered symmetrically from one end of the compounds to the other, *i.e.* Cl to Cl atoms. Hydrogen atoms are omitted for clarity. Magenta lines indicate the π-boundaries of the donor (D) and acceptor (A) moieties

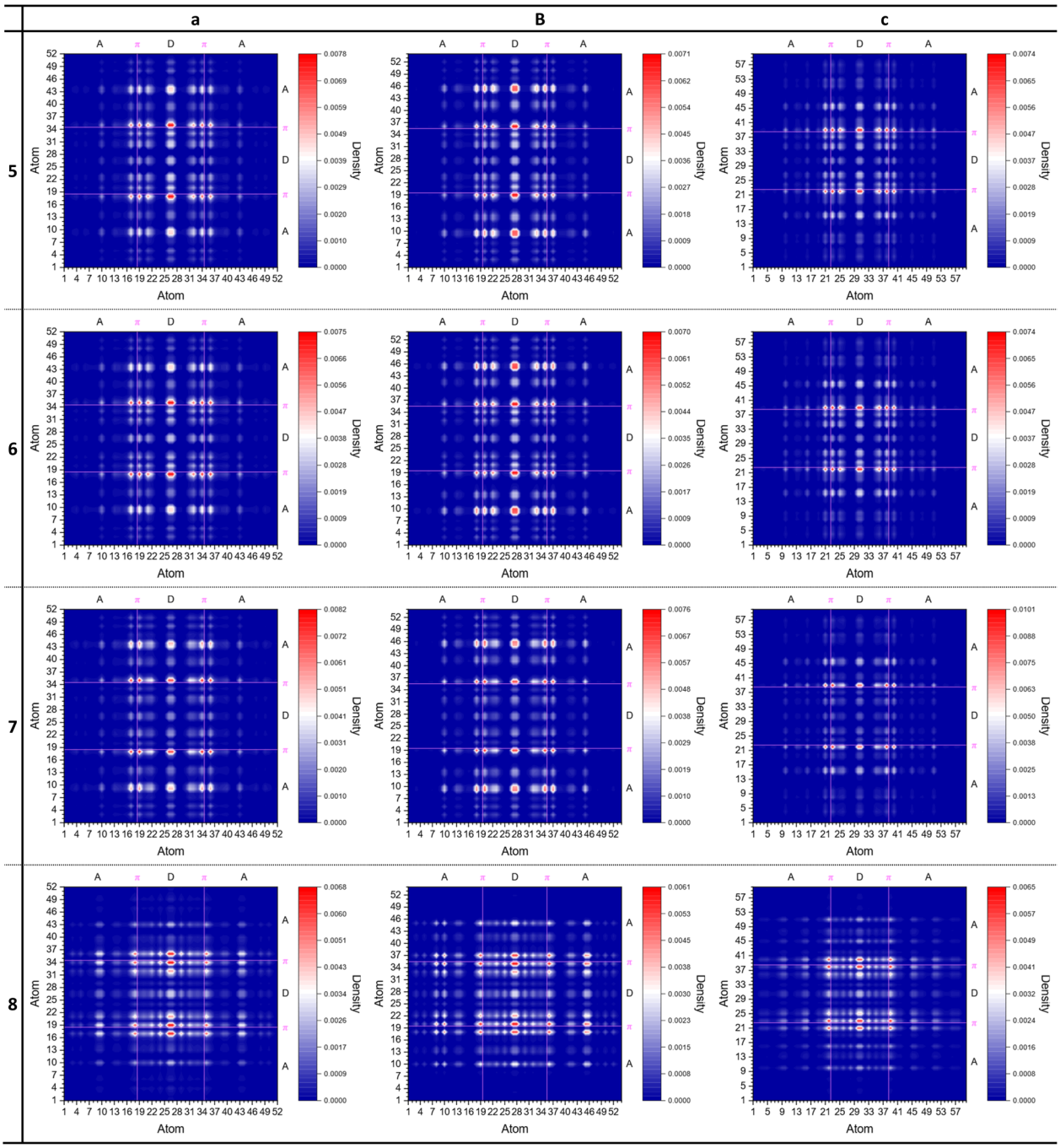

smaller scale when compared to the third group. For these six compounds, the matrices reveal very similar profiles among **5**, **6** and **7** compounds, suggesting no noticeable influence of the donor moiety.

In contrast, comparisons between **a** and **b** moieties consistently show more significant charge transfer for the latter. Indeed, the density spots around lines 9 and 10 are higher when the sulfonated acceptor **b** is used. To quantitatively support the qualitative observations made from the CTMs, the inter-fragmentary charge transfer (IFCT) calculation was performed. This method allows for an accurate determination of the electron density transferred from the donor moiety to the acceptor moieties (see SI, for more computational details). Consistent with the CTM analysis, the compounds incorporating donor and acceptor moieties with the weakest charge transfers are **8** and **c**, respectively (Fig. 8).

© 2025 The Author(s). Published by the Royal Society of Chemistry

Open Access Article. Published on 11 November 2025. Downloaded on 5/1/2026 8:46:12 AM. This article is licensed under a Creative Commons Attribution-NonCommercial 3.0 Unported Licence.

Specifically, the average values obtained for the donor and acceptor moieties yield the following rankings: **8** (0.0695) << **6** (0.2654) < **5** (0.2770) < **7** (0.3323) for donor moieties and **c** (0.1986) < **a** (0.2321) < **b** (0.2775) for acceptor moieties. Thus, donor moieties **5** and **6**, along with acceptor moiety **a**, show promising values, while the nitrogenated donor **7** and the sulfonated acceptor **b** stand out presenting the highest overall IFCT.

Moreover, it is particularly noteworthy to observe the significant impact of the additional double bond in the donor moiety **8** compared to **7**. This subtle modification positions them as polar opposites in terms of charge transfer property as evaluated by this methodology. Referring to the FMOs of compounds **8a–c** previously analysed, it can be inferred that the concentration of electron density on the central donor moiety in both the HOMO and LUMO likely hinders the desired charge transfer between the donor and acceptor moieties.

Reorganization energy. When the charges of the exciton are separated, the ability of the donor and acceptor materials in the active layer to transport these charges stands as a critical aspect. This capability is essential for minimizing energy losses due to recombination processes and enhancing charge collection efficiency at the electrodes.[68] Specifically, at the OPV cell scale, NFAs are responsible for capturing electrons from the donor material and are therefore expected to exhibit high electron mobility. From a computational perspective, one method commonly used to predict this property is the calculation of reorganization energy (λ_e, SI, for methodology details).[69,70] Briefly, reorganization energy refers to the energy difference between the geometries of the neutral species and its negatively charged radical counterpart. An inverse correlation is observed between λ_e and electron mobility, *i.e.* the lower the λ_e value, the smaller the geometric change, allowing the NFA to more easily accept an additional electron and, consequently, facilitate its transport. For the studied compounds, the average reorganization energy values, categorized by donor and acceptor moieties, yield the following rankings: **b** (0.2461) < **a** (0.2577) << **c** (0.4997) for acceptors and **7** (0.2895) < **6** (0.3232) < **5** (0.3563) < **8** (0.3690) for donors (Fig. 9).

With an average λ_e almost twice as high as those observed for the carbonyl- and sulfonate-containing acceptors **a** and **b**, the bis-malononitrile functionalized acceptor c appears to hinder electron mobility. From the donor perspective, the fully conjugated sulphur-based (**5**) and nitrogen-based (**8**) moieties exhibit the highest reorganization energies, marking them as the least efficient for electron mobility. In contrast, the oxygenated donor **6** and the carbonyl acceptor a demonstrate relatively intermediate values, suggesting moderately promising performance. Finally, the nitrogen-based donor **7** and the sulfonated acceptor **b** once again emerge as the most promising moieties for the studied property, electron mobility.

Comparative study with the Y6 archetype

In an OPV cell, the key performance parameters are the short-circuit current density (J_{sc}), the open-circuit voltage (V_{oc}), and the fill factor (FF), which collectively determine the power conversion efficiency (PCE). These parameters are directly influenced by the interaction and compatibility of the donor and acceptor materials in the active layer. Through computational modelling, it becomes possible to estimate certain properties, such as the λ_{max} and FMOs, which can be used as indicators of key performance metrics. To qualitatively assess the relevance of our studied compounds, we focus on the well-known **Y6** molecule, a benchmark in the field of OPVs that has achieved record-breaking PCEs, particularly when using its derivatives.[71–73] To ensure a relevant comparison and given that the **Y6** molecule closely resembles our studied compounds in terms of atomic composition and heteroatom distribution, we applied our computational methodology to determine its λ_{max}, f, and IFCT, as well as the energy levels of its FMOs and λ_e (see SI, for detailed values). The studied compounds were compared to **Y6** based on these six key parameters, leading to the

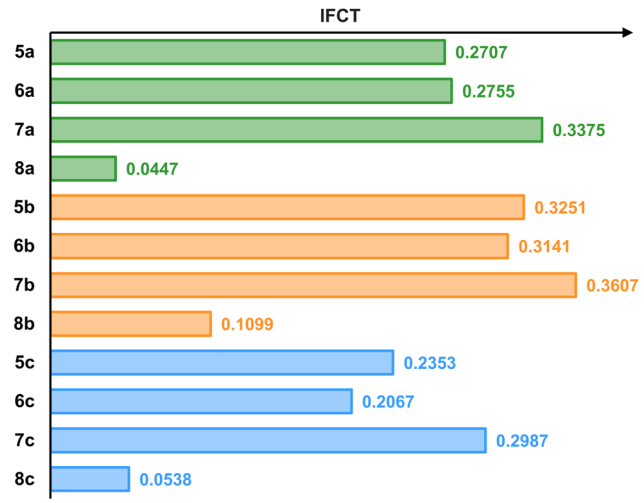

Fig. 8 Calculated interfragmentary charge transfer (IFCT) occurring for each compound from the central donor moiety to the two adjacent acceptor moieties.

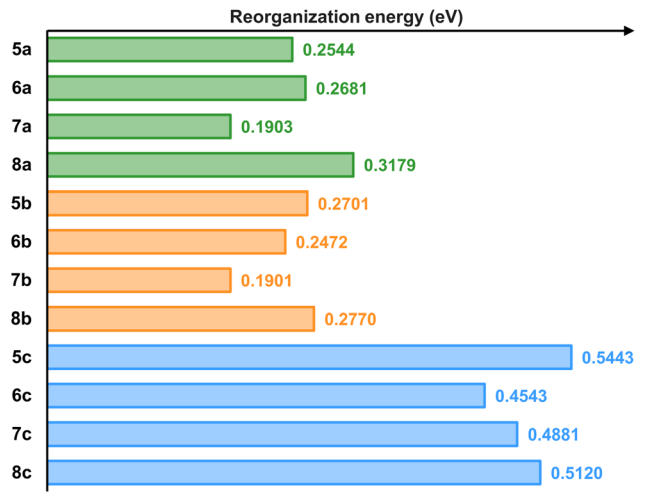

Fig. 9 Calculated reorganization energies relative to electron transport (λ_e) of all compounds.

© 2025 The Author(s). Published by the Royal Society of Chemistry

Open Access Article. Published on 11 November 2025. Downloaded on 5/1/2026 8:46:12 AM.
This article is licensed under a Creative Commons Attribution-NonCommercial 3.0 Unported Licence.

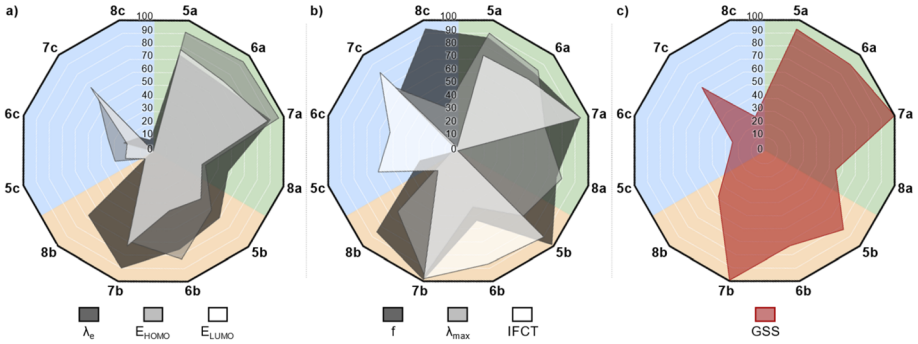

Fig. 10 Radar plots of the similarity of studied compounds and **Y6** in terms of (a) electronic properties, (b) photophysical properties and (c) global similarity score.

establishment of individual similarity scores (SS) as well as a Global Similarity Score (GSS) to highlight the most relevant candidates. Briefly, for each parameter, a score of 100 corresponds to the **Y6** reference value, while a score of 0 is assigned to the compound with the most divergent value. The GSS is then calculated as the average of the six individual scores, normalized with respect to the highest observed mean score. The outcomes of this comparison are represented through three radar plots reported in Fig. 10 (see SI, for detailed methodology) where compounds are grouped according to the type of acceptor moiety **a**, **b**, and **c** corresponding to the green, orange and blue regions, respectively. The first radar plot, associated with electronic properties (λ_e, E_{HOMO}, and E_{LUMO}), reveals that compounds bearing the acceptor moiety c generally display results furthest from the **Y6** reference, with the notable exception of compound **7c**, which emerges as the best performer within this group (Fig. 10a). Compounds with the **b** acceptor moiety show intermediate similarity, while **7b** stands out for its excellent reorganization energy score (90) and FMO energy levels scoring above or equal to 70. Among the compounds bearing acceptor moiety a, **5a**, **6a**, and **7a** exhibit the highest similarity scores, with E_{HOMO} scores above 90 and E_{LUMO} and λ_e values above or equal to 70. Notably, compound **7a** appears to display electronic properties most closely aligned with those of **Y6**. Regarding photophysical properties (f, λ_{max}, and IFCT), represented in the second radar plot, compound **7b** emerges as the closest analogue to **Y6**, achieving similarity scores of 99, 96, and 98 for oscillator strength, maximum absorption wavelength, and intramolecular charge transfer, respectively. Several other compounds also demonstrate strong performance in terms of oscillator strength (f), particularly **7a**, **5b**, and **8c**, all scoring above 90. For λ_{max}, compounds within group **a** (**5a**, **6a**, and **8a**) achieve scores above or equal to 80. Intermediate scores, ranging from 40 to 70, are observed for **7a**, **5b**, **8b**, and **7c**, whereas compounds **5c**, **6c**, and **8c** show the weakest performance. For charge transfer capability (IFCT), compounds **7a** and **5b** again score above 90, followed by **6b** and **7c** with respectable scores of 87 and 82, respectively. Finally, when considering the GSS as a comprehensive measure of similarity, compounds incorporating the nitrogen-based donor core **3** are consistently the most promising across all acceptor moiety groups, particularly compounds **7a** and **7b**, which achieve GSS values of 100 and 99, respectively. Compound **7a** demonstrates superior performance in terms of electronic properties, while **7b** excels in the photophysical domain. In contrast, compounds incorporating donor core **4** show the lowest similarity scores across all acceptor groups, with GSS values of 55, 48, and 26 for **8a**, **8b**, and **8c**, respectively – indicating that the fully π-conjugated nitrogen core tends to negatively affect most properties compared to **Y6**. A similar trend is observed for compounds incorporating acceptor moiety **c**. Nevertheless, compounds **5b** and **6b** show relatively promising GSS values of 83 and 73, while **5a** and **6a** perform even better with scores of 93 and 90, respectively.

Conclusions

Building upon previous computational investigations centred on novel donor moieties derived from BTDE, the present study aimed to explore the evolution of their optoelectronic properties through the incorporation of diverse acceptor moieties in the design of NFAs for OPV applications. Specifically, we assessed (i) the planarity and aromaticity of the compounds, (ii) the energy levels of their frontier molecular orbitals, (iii) their maximum absorption wavelengths, (iv) their intramolecular charge transfer capabilities, and (v) their reorganization energies, as indicators of electron mobility. From the comprehensive analysis of the influence of donor and acceptor moieties on the investigated properties, the nitrogen-containing donor moiety **3** and the sulfonyl acceptor moiety **b** emerged as the most promising structural units. These motifs were found to promote efficient π-conjugation (as evidenced by BLA values), enhanced charge transfer (IFCT), and favourable electron transport properties (low λ_e). Moreover, the incorporation of the sulfonyl acceptor b was associated with near-infrared λ_{max} values combined with relatively high oscillator strengths, which is advantageous for light harvesting. More specifically, the comparative evaluation against the archetype NFA **Y6** – based on six key parameters – identified compounds **7a** and **7b** as the most promising candidates, followed closely by **5a** and **6a**. These compounds exhibit a favourable balance of photophysical and electronic properties. These promising results will serve to guide future experimental synthesis efforts toward the aforementioned four compounds. Beyond assessing their photovoltaic performance

Open Access Article. Published on 11 November 2025. Downloaded on 5/1/2026 8:46:12 AM. This article is licensed under a Creative Commons Attribution-NonCommercial 3.0 Unported Licence.

as NFAs in OPV devices, it will also be essential to validate the accuracy of the computational methods employed. In particular, benchmarking calculated values such as IFCT and λ_e against experimental data will be critical for refining our predictive capabilities. The more experimental data we acquire, the better we can calibrate our database and enhance the robustness of our computational methodologies.

Author contributions

J. G.: investigation, methodology, visualization, formal analysis, writing-original draft, writing-review; T. N.: investigation, visualization, formal analysis, writing-review; J. M. S.: resources, supervision, validation, writing review; J.-M. R.: conceptualization, supervision, validation, methodology, project administration, writing original draft, review & editing.

Conflicts of interest

There are no conflicts to declare.

Data availability

The data supporting this article have been included a part of the supporting information (SI). Supplementary information: the SI provides computational methodologies, atom indexation, charge transfer and reorganization energy schemes, along with calculated electronic and photophysical properties, similarity scores, optimized structures, FMOs, absorption spectra and Cartesian coordinates. See DOI: **https://doi.org/10.1039/d5ra04742k**.

Acknowledgements

This work was supported by the Centre National de la Recherche Scientifique (CNRS) and the ministère de l'Enseignement Supérieur et de la Recherche (MESR). T. M. and J.-M. R also acknowledge the AMUTech institute. MCIA (Mesocentre de Calcul Intensif Aquitain) is gratefully acknowledged for calculation facilities.

Notes and references

1 G. Wang, F. S. Melkonyan, A. Facchetti and T. J. Marks, *Angew. Chem., Int. Ed.*, 2019, **58**, 4129–4142.
2 S. Yuvaraja, A. Nawaz, Q. Liu, D. Dubal, S. G. Surya, K. N. Salama and P. Sonar, *Chem. Soc. Rev.*, 2020, **49**, 3423–3460.
3 S. Jadoun and U. Riaz, in *Polymers for Light-Emitting Devices and Displays*, ed. Inamuddin, R. B., M. I. Ahamed, A. M. Asiri, Wiley, Hoboken, 2020, pp. 77–98.
4 H. Mandal, O. J. Ogunyemi, J. L. Nicholson, M. E. Orr, R. F. Lalisse, A. Rentería-Gómez, A. R. Gogoi, O. Guitierrez, Q. Michaudel and T. Goodson III, *J. Phys. Chem. C*, 2024, **128**, 2518–2528.
5 H. Yanai, Y. Terajima, F. Kleemiss, S. Grabowsky and T. Matsumoto, *Chem. Eu. J.*, 2023, **29**, e202203538.
6 B. Matarranz, G. Ghosh, R. Kandeanelli, A. Sampedro, K. K. Kartha and G. Fernández, *Chem. Commun.*, 2021, **57**, 4890–4893.
7 Y. Nakakuki, T. Hirose, H. Sotome, M. Gao, D. Shimizu, R. Li, J.-Y. Hasegawa, H. Miyasaka and K. Matsuda, *Nat. Commun.*, 2022, **13**, 1475.
8 N. K. Kalinichenko, D. O. Balakirev, P. S. Savchenko, A. L. Mannanov, S. M. Peregudova, D. Y. Paraschuk, S. A. Ponomarenko and Y. N. Luponosov, *Dyes Pigm.*, 2021, **194**, 109592.
9 V. Malytski, J.-J. Simon, L. Patrone and J. M. Raimundo, *RSC Adv.*, 2015, **5**, 354–397.
10 M. Tonga, *Tetrahedron Lett.*, 2020, **61**, 152205.
11 A. Tang, P. Cong, T. Dai, Z. Wang and E. Zhou, *Adv. Mater.*, 2024, **36**, 2300175.
12 M. Klikar, P. Solanke, J. Tydlitát and F. Bureš, *Chem. Rec.*, 2016, **16**, 1886–1905.
13 F. Bureš, *RSC Adv.*, 2014, **4**, 58826–58851.
14 P. Kaur and K. Singh, *Chem. Rec.*, 2022, **22**, e2022200024.
15 B. Milián-Medina and J. Gierschner, *Wiley Interdiscip. Rev. Comput. Mol. Sci.*, 2012, **2**, 513–524.
16 C. Pigot, D. Brunel and F. Dumur, *Molecules*, 2022, **27**, 5976.
17 C. Yan, *Green Synth. Catal.*, 2023, **4**, 78–88.
18 J.-M. Raimundo, P. Blanchard, P. Frère, N. Mercier, I. Ledoux-Rack, R. Hierle and J. Roncali, *Tetrahedron Lett.*, 2001, **42**, 1507–1510.
19 A. R. Morales, A. Frazer, A. W. Woodward, H.-Y. Ahn-White, A. Fonari, P. Tongwa, T. Timofeeva and K. D. Belfield, *J. Org. Chem.*, 2013, **78**, 1014–1025.
20 R. Nishiyabu and P. Azenbacher Jr, *Org. Lett.*, 2006, **8**, 359–362.
21 F. A. M. Al-Zahrani, R. M. El-Shishtawy, A. M. Asiri, A. M. Al-Soliemy, K. A. Mellah, N. S. E. Ahmed and A. Jedidi, *BMC Chem.*, 2020, **14**, 1–11.
22 P. E. Martin Varguez and J.-M. Raimundo, *Biosensors*, 2022, **12**, 407.
23 J. Zhang, H. S. Tan, X. Guo, A. Facchetti and H. Yan, *Nat. Energy*, 2018, **3**, 720–731.
24 R. D. Maduwu, H. C. Jin and J. H. Kim, *Macromol. Res.*, 2019, **27**, 1261–1267.
25 H. Feng, N. Qiu, X. Wang, Y. Wang, B. Kan, X. Wan, M. Zhang, A. Xia, C. Li, F. Liu, H. Zhang and Y. Chen, *Chem. Mater.*, 2017, **29**, 7908–7917.
26 J. Huang, H. Tang, C. Yan and G. Li, *Cell. Rep. Phys. Sci.*, 2021, **2**, 100292.
27 S. Baik, D. W. Kim, H.-S. Kang, S. H. Hong, S. Park, B.-K. An and S. Y. Park, *Sustain. Energ. Fuels*, 2022, **6**, 110–120.
28 Y. Zhang, Y. Lang and G. Li, *EcoMat*, 2023, **5**, e12281.
29 E. D. Papkovskaya, D. O. Balakirev, J. Min and Y. N. Luponosov, *Mater. Today Energy*, 2024, **43**, 101591.
30 A. Mahmood, J. Yang, J. Hu, X. Wang, A. Tang, Y. Geng, Q. Zeng and E. Zhou, *J. Phys. Chem. C*, 2018, **122**, 29122–29128.
31 S. Rasool, J. Yeop, H. W. Cho, W. Lee, J. W. Kim, D. Yuk and J. Y. Kim, *Mater. Futures*, 2023, **2**, 032102.
32 K. Liu, Y. Jiang, G. Ran, F. Liu, W. Zhang and X. Zhang, *Joule*, 2024, **8**, 835–851.

© 2025 The Author(s). Published by the Royal Society of Chemistry

Open Access Article. Published on 11 November 2025. Downloaded on 5/1/2026 8:46:12 AM. This article is licensed under a Creative Commons Attribution-NonCommercial 3.0 Unported Licence.

33 P. Blanchard, P. Verlhac, L. Michaux, P. Frere and J. Roncali, *Chem. Eu. J.*, 2006, **12**, 1244–1255.
34 H. Brisset, S. Le Moustarder, P. Blanchard, B. Illien, A. Riou, J. Orduna, J. Garin and J. Roncali, *J. Mater. Chem. C*, 1997, **7**, 2027–2032.
35 P. Blanchard, H. Brisset, B. Illien, A. Riou and J. Roncali, *J. Org. Chem.*, 1997, **62**, 2401–2408.
36 T. Benincori, E. Brenna, F. Sannicolo, L. Trimarco, G. Schiavon, S. Zecchin and G. Zotti, *Macromol. Chem. Phys.*, 1996, **197**, 517–528.
37 J. Roncali, C. Thobie-Gautier, E.-H. Elandaloussi and P. Frere, *J. Chem. Soc., Chem. Commun.*, 1994, **19**, 2249–2250.
38 J.-M. Raimundo, P. Blanchard, N. Gallego-Planas, N. Mercier, I. Ledoux-Rak, R. Hierle and J. Roncali, *J. Org. Chem.*, 2002, **67**, 205–218.
39 J.-M. Raimundo, P. Blanchard, L. Michaux, J. Roncali, I. Ledoux-Rak and R. Hierle, *Chem. Commun.*, 2000, **17**, 1597–1598.
40 C. Zhu, A. J. Kalin and L. Fang, *Acc. Chem. Res.*, 2019, **52**, 1089–1100.
41 A. Takai, Z. Chen, X. Yu, N. Zhou, T. J. Marks and A. Facchetti, *Chem. Mater.*, 2016, **28**, 5772–5783.
42 J. Garo, T. Nicolini, J. M. Sotiropoulos and J.-M. Raimundo, *Chem. Eur. J.*, 2024, **30**, e202402461.
43 Y. Cui, C. Yang, H. Yao, J. Zhu, Y. Wang, G. Jia, F. Gao and J. Hou, *Adv. Mater.*, 2017, **29**, 1703080.
44 P. Hohenberg and W. Kohn, *Phys. Rev.*, 1964, **136**, B864–B871.
45 W. Kohn and L. J. Sham, *Phys. Rev.*, 1965, **140**, A1133–A1138.
46 E. Runge and E. K. U. Gross, *Phys. Rev. Lett.*, 1984, **52**, 997–1000.
47 M. J. Frisch, G. W. Trucks, H. B. Schlegel, G. E. Scuseria, M. A. Robb, J. R. Cheeseman, G. Scalmani, V. Barone, G. A. Petersson, H. Nakatsuji, X. Li, M. Caricato, A. V. Marenich, J. Bloino, B. G. Janesko, R. Gomperts, R. Mennucci, H. P. Hratchian, J. V. Ortiz, A. F. Izmaylov, J. L. Sonnenberg, D. Williams-Young, F. Ding, F. Lipparini, F. Egidi, J. Goings, B. Peng, A. Petrone, T. Henderson, D. Ranasinghe, V. G. Zakrzewski, J. Gao, N. Rega, G. Zheng, W. Liang, M. Hada, M. Ehara, K. Toyota, R. Fukuda, J. Hasegawa, M. Ishida, T. Nakajima, Y. Honda, O. Kitao, H. Nakai, T. Vreven, K. Throssel, J. A. Montgomery, Jr., J. E. Peralta, F. Ogliar, M. J. Bearpark, J. J. Heyd, E. N. Brothers, K. N. Kudin, V. N. Staroverov, T. A. Keith, R. Kobayashi, J. Normand, K. Raghavachari, A. P. Rendell, J. C. Burant, S. S. Iyengar, J. Tomasi, M. Cossi, J. M. Millam, M. Klene, C. Adamo, R. Cammi, J. W. Ochterski, R. L. Martin, K. Morokuma, O. Farkas, J. B. Foresman and D. J. Fox, *Gaussian 16, Revision C.01*, Gaussian Inc., Wallingford, CT, 2016.
48 S. H. Vosko, L. Wilk and M. Nusair, *Can. J. Phys.*, 1980, **58**, 1200.
49 A. D. Becke, *J. Chem. Phys.*, 1993, **98**, 5648–5652.
50 P. J. Stephens, F. J. Devlin, C. F. Chabalowski and M. J. Frisch, *J. Phys. Chem.*, 1994, **98**, 11623–11627.
51 C. Lee, W. Yang and R. G. Parr, *Phys. Rev. B*, 1988, **37**, 785–789.
52 S. Grimme, J. Anthony, S. Ehrlich and H. Krieg, *J. Chem. Phys.*, 2010, **132**, 1–19.
53 S. Grimme, S. Ehrlich and L. Goerigk, *J. Comput. Chem.*, 2011, **32**, 1456–1465.
54 R. Krishnan, J. S. Binkley, R. Seeger and J. A. Pople, *J. Chem. Phys.*, 1980, **72**, 650–654.
55 T. Clark, J. Chandrasekhar, G. W. Spitznagel and P. V. R. Schleyer, *J. Comput. Chem.*, 1983, **4**, 294–301.
56 T. Lu and F. Chen, *J. Comput. Chem.*, 2012, **33**, 580–592.
57 T. Lu, *J. Chem. Phys.*, 2024, **161**, 082503.
58 G. A. Zhurko, Chemcraft., can be found under **http://www.chemcraftprog.com/**, 2005, accessed: 1 Apr 2025.
59 J.-C. Florès, M.-A. Lacour, X. Sallenave, F. Serein-Spirau, J.-P. Lère-Porte, J. J. E. Moreau, K. Miqueu, J.-M. Sotiropoulos and D. Flot, *Chem. Eur. J.*, 2013, **19**, 7532–7546.
60 V. Kojasoy and D. J. Tantillo, *Org. Biomol. Chem.*, 2023, **21**, 11–23.
61 B. M. Wood, A. C. Forse and K. A. Persson, *J. Phys. Chem. C*, 2020, **124**, 5608–5612.
62 D. Jacquemin, E. A. Perpète, H. Chermette, I. Ciofini and C. Adamo, *Chem. Phys.*, 2007, **332**, 79–85.
63 M. Kim, S. U. Ryu, S. A. Park, Y.-J. Pu and T. Park, *Chem. Sci.*, 2021, **12**, 14004–14023.
64 A. Classen, C. L. Chochos, L. Lüer, V. G. Gregoriou, J. Wortmann, A. Osvet, K. Forberich, I. McCulloch, T. Heumüller and C. J. Brabec, *Nat. Energy*, 2020, **5**, 711–719.
65 B. Lu, J. Wang, Z. Zhang, J. Wang, X. Yuan, Y. Ding, Y. Wang and Y. Yao, *Nano Select*, 2021, **2**, 2029–2039.
66 D. Luo, L. Zhang, J. Zeng, W. Chi, J. Zhou, E. Zhou, L. Li, T. Iwahashi, T. Michinobu, Y. Ouchi, B. Xu and A. K. K. Kyaw, *Adv. Funct. Mater.*, 2023, **34**, 2311736.
67 S. Giannini, D. J. C. Sowood, J. Cerdá, S. Frederix, J. Grüne, G. Londi, T. Marsh, P. Ghosh, I. Duchemin, N. C. Greenham, K. Vandewal, G. D'Avino, A. J. Gillett and D. Beljonne, *Mater. Today*, 2024, **80**, 308–326.
68 D. Bartesaghi, I. D. C. Pérez, J. Kniepert, S. Roland, M. Turbiez, D. Neher and L. J. A. Koster, *Nat. Commun.*, 2015, **6**, 7083.
69 S. Ahmed, I. Irshad, S. Nazir, S. Naz, M. A. Asghar, S. M. Alshehri, S. Bullo and M. L. Sanyang, *Sci. Rep.*, 2023, **13**, 15064.
70 T. Hassan, I. Sajid, M. Ramzan Saeed Ashraf Janjua, Z. Shafiq, M. Yasir Mehboob and N. Sultan, *Comput. Theor. Chem.*, 2023, **1224**, 114128.
71 J. Yuan, Y. Zhang, L. Zhou, G. Zhang, H.-L. Yip, T.-K. Lau, X. Lu, C. Zhu, H. Peng, P. A. Johnson, M. Leclerc, Y. Cao, J. Ulanski, Y. Li and Y. Zou, *Joule*, 2019, **3**, 1140–1151.
72 L. Zhu, M. Zhang, G. Zhou, Z. Wang, W. Zhong, J. Zhuang, Z. Zhou, X. Gao, L. Kan, B. Hao, F. Han, R. Zeng, X. Xue, S. Xu, H. Jing, B. Xiao, H. Zhu, Y. Zhang and F. Liu, *Joule*, 2024, **8**, 3153–3168.
73 H. Chen, Y. Huang, R. Zhang, H. Mou, J. Ding, J. Zhou, Z. Wang, H. Li, W. Chen, J. Zhu, Q. Cheng, H. Gu, X. Wu, T. Zhang, Y. Wang, H. Zhu, Z. Xie, F. Gao, Y. Li and Y. Li, *Nat. Mater.*, 2025, **24**, 444–453.